

Changing nanoslot ion flux with a dynamic nanocolloid ion-selective filter: Secondary overlimiting currents due to nanocolloid-nanoslot interaction

Gilad Yossifon¹ and Hsueh-Chia Chang^{2,*}

¹Faculty of Mechanical Engineering, Micro- and Nanofluidics Laboratory, Technion-Israel Institute of Technology, Technion City 32000, Israel

²Department of Chemical and Biomolecular Engineering, Center for Microfluidics and Medical Diagnostics, University of Notre Dame, Notre Dame, Indiana 46556, USA

(Received 20 January 2010; revised manuscript received 13 May 2010; published 29 June 2010)

Nanocolloids trapped at the depleted side (anodic) of a fluidic nanoslot entrance are shown to sensitively regulate dc ion transport through the nanoslot, such that a second limiting-overlimiting transition occurs in its nonlinear current-voltage characteristics. The nanocolloids, brought to the entrance by electro-osmosis, are not stationary but are confined to closed circular and toroidal streamlines, driven by a back-pressure corner vortex and an orthogonal electroconvection vortex instability. The transition from the corner vortex to a complex torus with both vortical motions coincides with the first overlimiting transition, while electrostatic interaction of nanocolloids in these vortices with the nanoslot entrance drives the second limiting transition.

DOI: 10.1103/PhysRevE.81.066317

PACS number(s): 47.57.jd, 47.20.Ma, 47.61.Fg, 82.39.Wj

It has been shown in recent years that field-driven passage of a single biomolecule/nanobead through an artificial nanopore can produce detectable differences in the nanochannel dc conductance and ac capacitance [1], suggesting a sensitive molecular detection platform. A different detection platform involving nanocolloid assays has also shown promise, as molecular hybridization onto the nanocolloid significantly changes the surface conductance and the direction of the induced nanocolloid dipole [2,3]. Due to field focusing effects, the field in the nanopore is much higher than that in the microreservoir outside the pore. As such, hybridized nanocolloids may be preferentially attracted to the nanopores by dielectrophoresis (DEP)—a particle force due to induced particle dipoles. Alternatively, DEP sorters [4] can remove the unhybridized beads upstream and hybridized ones can be convected by electro-osmotic flow toward the nanochannels. Indeed, earlier work shows that, depending on the relative dimensions of the nanochannel cross section and nanocolloid size, the latter can be blocked at the nanochannel's entrance, translocate through the channel or aggregate within it [5]. We show in this letter that, under specific conditions, nanocolloids trapped at the entrance can produce the largest change in the conductance, and hence suggest a combination of these two platforms (nanocolloids DEP and dc nanochannel conductance or low-frequency impedance) for extremely sensitive and nonoptical nanocolloidal-based biomolecular detection [2,3].

Several characteristics of the nanochannel produce very sensitive ion-current dependence on the voltage that can be utilized to amplify the effects of nanocolloids on nanochannel conductance: ion-permselectivity [6] and the resulting ion enrichment/depletion [7], over-limiting current due to hydrodynamic vortices [8,9] and ionic current rectification [10]. While previous studies have focused on sensing the presence (or translocation) of the biomolecule/nanobead within the nanochannel under low voltage (i.e., Ohmic) conditions, we

demonstrate for the first time that, due to the depletion and hydrodynamic vortices, their presence at the nanochannel entrance under high-voltage (overlimiting) conditions produces far larger signals.

In our experiments, fluorescently tagged polystyrene nanocolloids (Duke Scientific Corporation) of varying size (larger or smaller than the nanoslot height) were used together with a wide nanoslot chip (inset of Fig. 1) whose fabrication details are described elsewhere [11] together with the channel cleaning, solution preparation and current-voltage (I - V) measurement procedures. Different dilutions of a 1 M potassium chloride (KCl) solution were used in order to change the ionic strength and control the degree of EDL (electric double layer) overlap or ion selectivity, as measured by relative dimension of the Debye screening length λ and the gap height h . That pronounced EDL overlap exists for electrolyte solution concentration of 0.1 mM, but not for 0.1 M, was already shown for the same chip in ([11], Fig. 1(b)). We hence choose, in the current study, to focus on these two extreme concentrations. That conduction effects through the body of the nanofluidic device, in particular through the intermediate polysilicon layer, can be discarded is supported by the agreement between the measured conductivity versus ionic concentration and the theoretical predictions for an identical device ([11], Fig. 1(b)).

A curious phenomenon is the appearance of a second limiting to overlimitinglike transition for the case of nanobeads of size larger than the nanoslot height (Fig. 1), resulting in a significantly smaller supercritical current. Also, a much larger threshold voltage for the overlimiting current (indicated in Fig. 1 by a second critical voltage $\sim 35\text{--}40$ V) occurs relative to the case of a suspensionless electrolyte solution (critical voltage ~ 15 V). In contrast, smaller nanocolloids (100 nm) that are able to pass freely through the nanoslot exhibit current-voltage characteristics similar to those of the suspensionless electrolyte except for a smaller limiting differential resistance. The latter can be explained by colloids (having the same surface negative charge sign as the

*Corresponding author; hchang@nd.edu

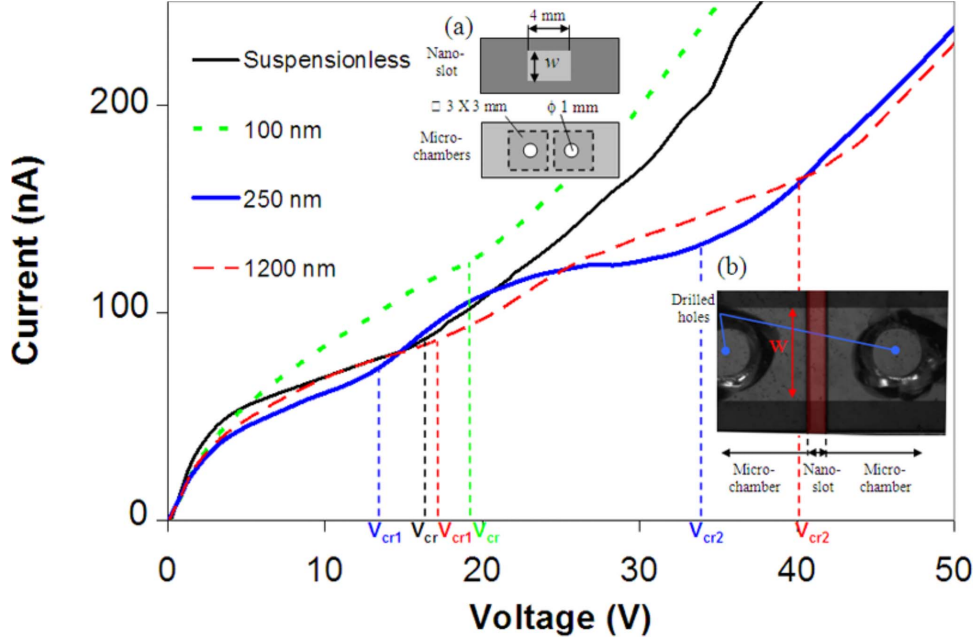


FIG. 1. (Color online) Current-voltage curves for 0.1 mM KCl electrolyte solution concentration for various nanobead diameters (designated by different colored lines) at 0.02% volumetric concentration. A curious second limiting to overlimitinglike transition (indicated by the second critical voltage V_{cr2}) occurs for nanobeads larger than the nanoslot height (190 nm). Inset: (a) schematic of the two Pyrex slides containing the chip. Top slide—rectangle of width $w=2.5$ mm and depth $h=190$ nm, that is etched into the deposited 190 nm thick polysilicon layer on top of a 1 mm Pyrex glass slide. Bottom slide—two square microchambers of 50 μm depth that were wet-etched into a second 1 mm Pyrex glass slide; (b) Optical microscope image (top view) of the chip with the nanoslot of 0.5 mm in length emphasized with red background.

channel wall) adsorbing onto the nanoslot walls to produce an increase in the effective surface charge density, and thus enhancing the counterions concentration and conductivity within the nanoslot. Due to EDL overlap, the counterions dominate within the nanoslot and control its overall current [6]. The presence of the nanocolloids themselves, freely suspended within the nanoslot volume, without adsorption cannot account for this increase of the channel conductivity due to their small volumetric concentration 0.02%. In contrast, adsorption is an accumulative process that may result in a significantly larger number of beads contained within the nanoslot to affect its overall conductance.

To understand the physical mechanisms underlying this phenomenon, fluorescent imaging microscopy is performed. At low voltages (5 V), below the first critical voltage (~ 15 V), and weak electrolytes (0.1 mM), a band of nanobeads is formed within the microchamber at the anodic side of the nanoslot, with the colloids seemingly oscillating in straight lines back and forth from the nanoslot entrance (Fig. 2, see also the video in the supplementary materials [12]). In contrast, for strong electrolyte (0.1 M), when the EDLs do not overlap, the nanobeads seem to accumulate at the nanoslot entrance (Fig. 3, see also the supplementary video [12]) without forming a band at any applied voltage. A reasonable explanation for the oscillating band at low ionic strengths is that the seemingly linear colloidal movement is actually a projection of a closed circular trajectory in a plane that is perpendicular to the plane of view as well to nanoslot/microchamber interface—with a vorticity direction parallel to the chip substrates. These vortices are distinct from two

others that we have studied: induced-charge electro-osmotic corner vortices near corners [13] and vortices driven by an extended polarized layer at a nanoslot entrance [9]. The induced charge corner vortices occur at all ionic strengths and hence are not related to the current ones, while the vortices driven by extended polarized layers also develop only at low ionic strengths. However, the vorticity direction of the current vortices is perpendicular to those driven by extended polarized layers at higher voltages [9]. The vortices must hence be driven by a new mechanism.

Vortices are not expected for standard linear electroosmosis, wherein the EDL is much thinner than the nanoslot gap and the flow streamlines coincides with the irrotational electric field lines, known often as a “similitude” condition [14]. Other necessary conditions for such similitude [14] include a quasisteady electric field, uniform fluid and electric properties and bounding solid walls that must have uniform surface charge, must be impermeable to flow, and must be electrically nonconducting relative to the fluid. Such similitude condition is demonstrated for a model micronanoslot junction in the Supplementary Materials [12] with a conformal map analysis [13(b),15] of both the electric and flow potential that satisfy the Laplace equation. It is hence expected that the strong electrolyte solution case, for which the EDL is thin, roughly obeys the similitude condition and indeed no vortices have been experimentally observed (Fig. 3). With the small volume fraction (0.02%) of the nanocolloids, it is also unlikely that the conductivity and potential gradients due to nanocolloid concentration difference in the two microreservoirs is sufficient to break the similitude.

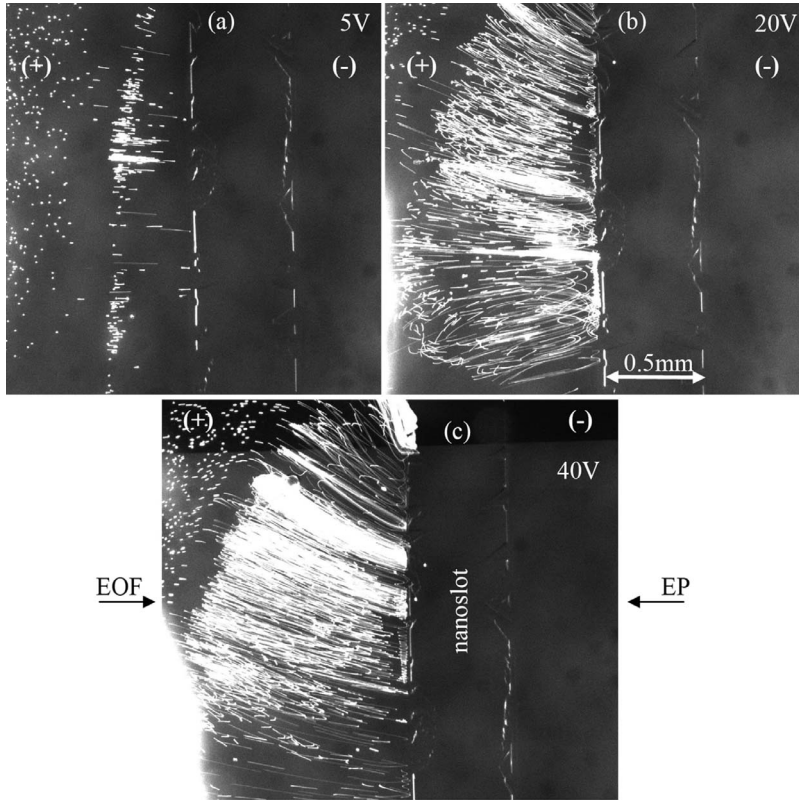


FIG. 2. Colloid dynamics for different applied voltages that are below (5 V), beyond (20 V) the first and beyond (40 V) the second critical voltages (see Fig. 1). The former exhibit linear colloid translations within the colloid band, while the two latter ones exhibit a complex toroidal movement. Furthermore, tangential motion of colloids trapped just at the nanoslot entrance becomes more pronounced with increased voltage. Nanocolloids ($1.2 \mu\text{m}$) larger than the nanoslot depth and weak electrolytes (0.1 mM) were used.

Breaking of the similitude conditions occurs when the EDLs are thicker than the nanoslot gap and the conductivity at the gap is different from the bulk, such that the velocity cannot be considered as a constant multiplicative factor of the electric field. In this case the space charge distribution in the nanochannel stipulates the potential satisfies the Poisson equation instead of the Laplace equation and the resulting bulk shear gradient stipulates that the Stokes equation is the relevant hydrodynamic equation. Following Burgreen (1964) [16], we use the one-dimensional Poisson-Boltzmann equation for the electric potential distribution, ϕ , between the two opposing channel surfaces (separated by h) with a Debye-Hückel simplification to produce

$$\phi(y) = \zeta^{eq} \cosh[\kappa(h/2 - y)]/\cosh(\kappa h/2), \quad (1)$$

where $\kappa = \lambda^{-1}$ is the reciprocal Debye length, ζ^{eq} is the natural zeta potential and y is the coordinate normal to the

channel wall ($y=0$). Considering the steady Stokes equation, while neglecting pressure gradients along the channel length (i.e., $dP/dx=0$), the x component of the velocity, satisfying the no-slip condition (i.e., $u=0$ at the surface) and $du/dy = d\phi/dy = 0$ at the center of the channel, can be shown to be

$$u = (\zeta^{eq} \varepsilon_0 \varepsilon_f / \mu) E_0 (1 - \phi/\zeta^{eq}), \quad (2)$$

wherein ε_0 is the dielectric permittivity of vacuum, ε_f is the dielectric constant of the fluid, μ is the fluid viscosity and E_0 is the uniform externally applied electric field within the nanochannel. Here, it was assumed that the externally applied potential Φ_f (associated with E_0) and that from the Debye layer, ϕ , can be superimposed. It is hence clear that the hydrodynamic resistance is increased with increasing EDL overlap (i.e., larger λ/h ratio). Qualitatively, the velocity profile shifts from a pluglike flow for $\lambda/h \ll 1$ to a forced Poiseuille-like flow for $\lambda/h \sim 1$ (supplementary Fig.S2 [12]).

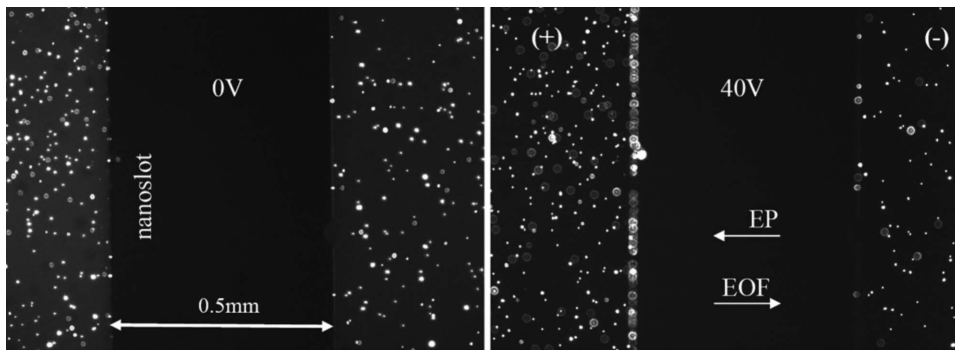


FIG. 3. Colloid dynamics for large colloids ($1.2 \mu\text{m}$) in strong electrolytes (0.1 M) before and after applying a 40 V voltage. In contrast to the weak electrolyte case, no colloid band is observed—the colloids accumulate instead at the nanoslot anodic entrance.

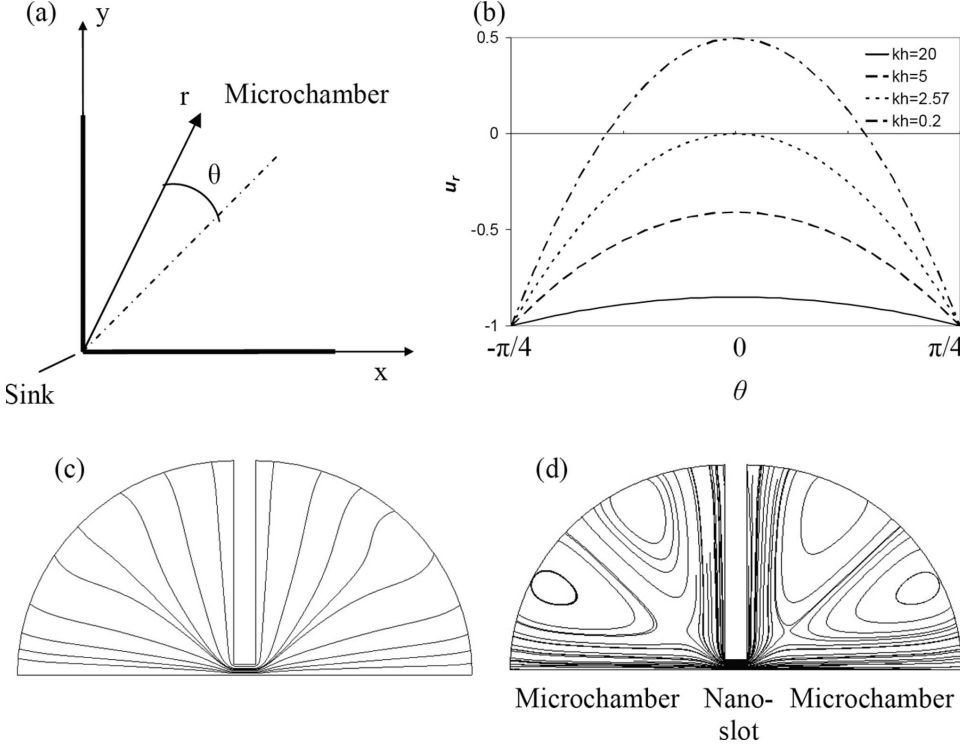


FIG. 4. (a) Schematics of the 90° wedge and sink simplifications of the micro- and nanochannel geometries, respectively; (b) Analytically calculated radial velocity [Eq. (5b)] versus θ for varying kh ratios; Numerically calculated velocity streamline for the case of (c) strong and (d) weak electrolytes for a model geometry.

We can model the flow in the microreservoir as a converging sink flow in a 90° wedge (Fig. 4(a)). In the microreservoir the thin EDL assumption holds. Hence, the electrostatic problem is obtained by solving the Laplace equation together with Neumann boundary conditions on the microchannel walls ($x=0, y=0$) and a sink of strength $m=2E_0h/\pi$ located at the origin ($x=y=0$), to yield a complex potential of the form $w=m \log z$, wherein $z=x+iy=re^{i\theta}$, and the resulting electric field components are $E_r=-m/r$ and $E_\theta=0$.

The stream function of the hydrodynamic problem satisfies the Stokes equation $\nabla^4\psi=0$ together with the requirements that

$$\psi=const \text{ at } \theta=\pm\pi/4, \quad (3a)$$

$$u_r=-\frac{1}{r}\frac{\partial\psi}{\partial\theta}=\frac{\zeta^{eq}\epsilon_0\epsilon_f}{\mu}\frac{1}{r}\frac{E_0h}{\pi/2} \text{ at } \theta=\pm\pi/4, \quad (3b)$$

and matching of the flux of this wedge flow to that in the nanoslot

$$\int_{-\pi/4}^{\pi/4} u_r r d\theta = -\psi|_{-\pi/4}^{\pi/4} = Q_{nanoslot}, \quad (4)$$

wherein $Q_{nanoslot}=\frac{\zeta^{eq}\epsilon_0\epsilon_f}{\mu}E_0h(1-\frac{\tanh(kh/2)}{kh/2})$, the flux through the nanoslot obtained by integrating Eq. (2). The Stokes equation admits the separation-of-variables solutions [17] $\psi=r^\mu f_\mu(\theta)$, where $f_\mu(\theta)=A\theta+B\theta^3$ for the particular case of $\mu=0$ [as obtained by satisfying Eq. (3)]. This solution contains a pressure-driven flow counter to the electro-osmotic flow because of the back pressure that builds up to ensure flow balance into the nanoslot. The resulting velocity components are

$$u_\theta=0, \quad (5a)$$

$$u_r=\frac{1}{\pi r}\left[2+3\frac{\tanh(kh/2)}{kh/2}\left(\left(\frac{4}{\pi}\right)^2\theta^2-1\right)\right]Q_{nanoslot}^0, \quad (5b)$$

where $Q_{nanoslot}^0=(\zeta^{eq}\epsilon_0\epsilon_f/\mu)E_0h$ is the electro-osmotic nanoslot flux in the limit of infinitesimally thin EDLs. The vortices appear at a critical λ/h ratio—where the minimum radial velocity component becomes negative [Fig. 4(b)]. Differentiating Eq. (5b) and equating to zero yields the critical ratio of $\lambda/h \sim 0.39$ which is close enough to the test conditions of the weak electrolyte $\lambda/h \sim 0.23$ (in contrast, for the strong electrolyte case $\lambda/h \sim 0.005$). This pressure-driven back flow in the microreservoir is responsible for the corner vortices with vorticity direction parallel to the chip substrates.

More explicit numerically computed (for more details see the supplementary materials [12]) streamlines for a simple model geometry of a nanoslot bounded by two microreservoirs is shown in Figs. 4(c) and 4(d). The occurrence of this corner vortex can be simply explained based on liquid flux continuity arguments. The irrotational electro-osmotic streamlines of strong electrolytes in Fig. 4(c) resemble those predicted analytically in the supplementary Fig. S1 [12].

At large voltage beyond the critical voltage for the suspensionless overlimiting current (~ 15 V), an electroconvection vortex instability of the depletion layer [18,9], with a vorticity direction perpendicular to the chip substrates, develops to produce a much more complex colloidal movement. Superposition of the vortex instability, in the lateral dimension (plane of view), with the vertical vortex occurring

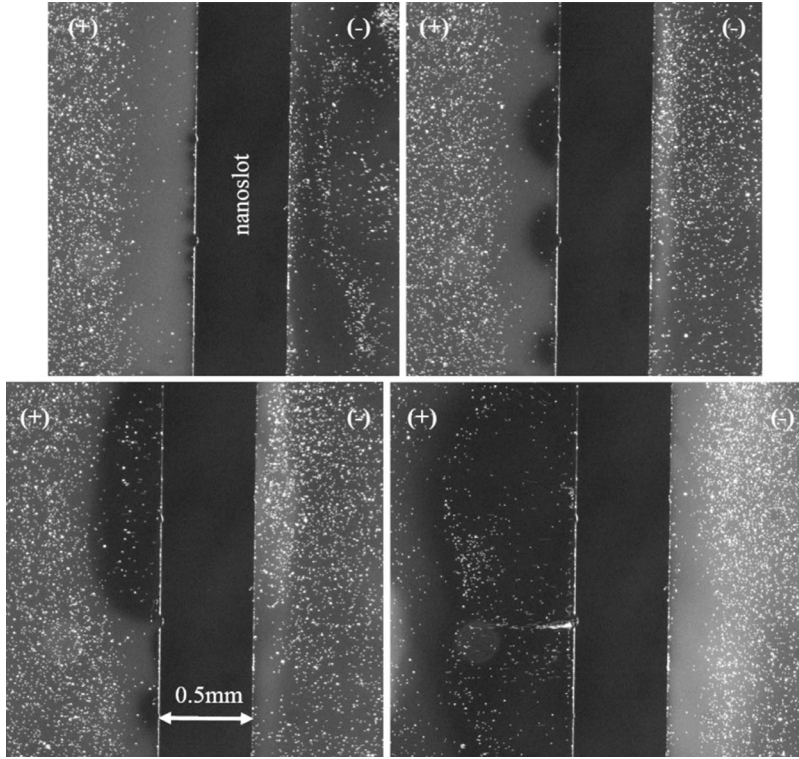


FIG. 5. Evolution of the depletion/enrichment regions of the fluorescently dyed electrolyte combined with the nanocolloids dynamics for a 30 V stepwise applied voltage. Nanocolloids ($1.2 \mu\text{m}$) larger than the nanoslot depth and weak electrolytes (0.1 mM) with Rhodamine 6 G ($10 \mu\text{M}$) were used.

in the orthogonal plane, yields a toroidal like particle streamlines as seen in Fig. 2 for the cases of 20 and 40 V. The emergence of this vortex instability explains the first inflection point (associated with the first critical voltage $\sim 15 \text{ V}$) of the I - V curve in Fig. 1, with or without nanocolloids.

If particle transport is by electrophoresis (EP) only, the negatively charged nanocolloids would accumulate only at the right entrance of the nanoslot in both Figs. 2 and 3, while the opposite is observed. Particle transport is hence predominantly by electro-osmotic flow (EOF) through the nanoslot. Dielectrophoretic trapping is also ruled out.

A possible explanation for the second limiting resistance-like region is the pronounced interaction of the colloids with the anodic nanoslot entrance (see Fig. 2 for 20 and 40 V and the supplementary videos [12]). Their presence can drive away coions and produce a second perm-selective (nanocolloidal based) membrane with its own limiting and over-limiting transition. Since this dynamic colloidal membrane form already in the depletion region of the first limiting-overlimiting transition, this second transition is on top of the first one. Importantly, this interaction is not stationary but rather a dynamic one wherein the colloids undergo either toroidal circulations following the instability induced vortices or tangential translations along the wide nanoslot entrance. The latter dynamics of the trapped nanocolloids is synchronized to the toroidal vortices whose circular convection also regulates their number.

Interestingly, the secondary limiting current is less pronounced for the larger beads ($1.2 \mu\text{m}$ relative to 250 nm , see Fig. 1) with a smaller particle density at the same volume fraction and whose larger crevices are not as ion selective. At any given time there is only a *partial* coverage of the nanoslot entrance by nanocolloids (see Fig. 2) and still their

presence strongly regulates the nanoslot current. It could be that partial coverage is enough to affect that overall nanoslot dc current, but it may also be that the nanocolloids dynamics, which increases with voltage, is such that the charge relaxation time is longer than the time interval between two successive nanocolloids visiting the same position in space along the nanoslot entrance, hence, resulting in a continuous repulsion of coions from the polarized layer, whose thickness l has been measured to be in excess of $100 \mu\text{m}$ at 20 V (Fig. 7 of [11]). The former time scale can be approximated as the ionic diffusion time across the extended space charge layer (i.e., polarized layer), that controls the overall current of the device, $l^2/D \sim 5 \text{ s}$, wherein the ionic diffusion coefficient is $D \sim 2 \times 10^{-9} \text{ m}^2/\text{s}$. The latter time scale, associated with the colloid dynamics, is faster than the microscopic image exposure time 0.3 s —it is apparent from Fig. 2(b) (20 V) that the nanocolloid trajectory path performs at least one complete circulation during the exposure time. It is also clear that at higher voltages the true time scales associated with the colloid movement are much smaller [Fig. 2(c) shows that there are several complete circulations of the nanocolloid trajectory path] as the nanocolloid velocity is nonlinearly dependent on the applied electric field. In contrast to this toroidal motion, the colloids also move tangentially along the micronanoslot interface. This tangential nanocolloid velocity is harder to estimate but it seems to be on the same order as the toroidal velocity. Beyond a critical voltage, the strong vortices eventually suppress the electro-osmotic flow responsible for colloidal accumulation at the nanoslot entrance, leading to a second critical voltage (~ 35 – 40 V) for the overlimiting current.

The transient response for the case of weak electrolyte upon a step increase of 30 V is shown in Fig. 5 (see also

the supplementary video [12]) where, in addition to the fluorescent nanobeads, fluorescent molecules (Rhodamine 6 G) were added to the electrolyte solution to observe the different enrichment/depletion regions. As can be clearly seen, the depletion layer is formed at the anodic side of the nanoslot through a complex process of wavelength selection. These depletion layers are associated with the occurrence of vortex instability and the onset of toroidal motion. On the opposite side, a uniform enrichment layer is formed, as can be expected, since there is no extended space charge with which instability can occur. Such enrichment/depletion regions were not obtained in the strong electrolyte case (Fig. 3), as expected, since no EDLs overlap leading to ion-permselectivity effect exists.

A desirable extension of the current contribution is to examine the case of nanocolloid-nanoslot interaction under alternating fields. Other than affecting ac dielectrophoresis for the nanocolloids, the ac field also allows the application of impedance spectroscopy techniques to measure nanocolloid capacitance and hence offers a quantification of the nanocolloid number.

G.Y. acknowledges support from the Taub Foundation. H.C.C. acknowledges support from NSF-IDBR Grant No. 0852741. We are grateful to Professor Y. Zhu and Professor A. Seabaugh of Notre Dame for the use of their equipment and for their advice and for the help of P. Mushenheim in obtaining the IV data.

-
- [1] O. A. Saleh and L. L. Sohn, *Nano Lett.* **3**, 37 (2003).
 - [2] H.-C. Chang, *AIChE J.* **53**, 2486 (2007).
 - [3] Z. Gagnon, S. Senapati, and H.-C. Chang, *Electrophoresis* **29**, 4808 (2008); S. Basuray and H.-C. Chang, *Biomicrofluidics* **4**, 013205 (2010).
 - [4] I.-F. Cheng, H.-C. Chang, D. Hou, and H.-C. Chang, *Biomicrofluidics* **1**, 021503 (2007).
 - [5] H.-C. Chang and G. Yossifon, *Biomicrofluidics* **3**, 012001 (2009).
 - [6] D. Stein, M. Kruithof, and C. Dekker, *Phys. Rev. Lett.* **93**, 035901 (2004).
 - [7] Q. Pu, J. Yun, H. Temkin, and S. Liu, *Nano Lett.* **4**, 1099 (2004).
 - [8] S. J. Kim, Y. C. Wang, J. H. Lee, H. Jang, and J. Han, *Phys. Rev. Lett.* **99**, 044501 (2007).
 - [9] G. Yossifon and H.-C. Chang, *Phys. Rev. Lett.* **101**, 254501 (2008); S. M. Rubinstein, G. Manukyan, A. Staicu, I. Rubinstein, B. Zaltzman, R. G. H. Lammertink, F. Muggele, and M. Wessling, *ibid.* **101**, 236101 (2008).
 - [10] G. Yossifon, Y. C. Chang, and H.-C. Chang, *Phys. Rev. Lett.* **103**, 154502 (2009).
 - [11] G. Yossifon, P. Mushenheim, Y.-C. Chang, and H.-C. Chang, *Phys. Rev. E* **81**, 046301 (2010).
 - [12] See supplementary material at <http://link.aps.org/supplemental/10.1103/PhysRevE.81.066317> for supplementary materials and videos.
 - [13] (a) S. K. Thamida and H. C. Chang, *Phys. Fluids* **14**, 4315 (2002); (b) G. Yossifon, I. Frankel, and T. Miloh, *Phys. Fluids* **18**, 117108 (2006).
 - [14] E. B. Cummings, S. K. Griffiths, R. H. Nilson, and P. H. Paul, *Anal. Chem.* **72**, 2526 (2000).
 - [15] L. M. Milne-Thomson, *Theoretical Hydrodynamics* (Macmillan, London, 1968).
 - [16] D. Burgreen and F. R. Nakache, *J. Phys. Chem.* **68**, 1084 (1964).
 - [17] H. K. Moffatt, *J. Fluid Mech.* **18**, 1 (1964).
 - [18] I. Rubinstein and B. Zaltzman, *Phys. Rev. E* **62**, 2238 (2000).